Proceedings of DETC'04
2004 ASME Design Engineering Technical Conferences
Salt Lake City, Utah, USA, September-October 28-2, 2004

DETC2004-57406

A PARALLEL 5 DOF POSITIONER FOR SEMI-SPHERICAL WORKSPACES

Benjamin Maurin, Bernard Bayle
Jacques Gangloff, Michel de Mathelin
LSIIT (UMR CNRS-ULP 7005), Strasbourg I University
Bd. S. Brant, BP 10413, 67412 Illkirch cedex, FRANCE
Email: maurin@eavr.u-strasbg.fr

Olivier Piccin
LICIA(EA3434), INSA-Strasbourg
24, Bd de la Victoire, 67084 Strasbourg, FRANCE
Email: Olivier.Piccin@insa-strasbourg.fr

ABSTRACT

In this paper, a new five-degree-of-freedom parallel manipulator is described and modeled. This structure has been specially designed for medical applications that require in the same time mobility, compactness and accuracy around a functional point. The purpose of this robotic device is to help practitioners to perform accurate needle insertions while preserving them from harmful intra-operative X-ray imaging devices. The system is built from revolute joints, among which only five joints are actuated to convey the required five degrees of freedom to its moving platform. A numerical simulation of the workspace and a physical prototype are presented.

INTRODUCTION

Because surgery is changing very fast, new medical devices are always needed to solve difficult tasks. In medical care, percutaneous procedures are among the upcoming treatments that can help the patient to have faster recovery and less painful interventions. Such interventions are commonly used for therapy or diagnosis by radiologists [1]. They consist in inserting a needle in the body of a patient through an entry point on the skin. Because of positioning accuracy requirements, these interventions are often done with intra-operative X-ray imaging devices such as Computed Tomography scans (CT-scan). Thus the practitioner may be exposed to large amounts of X-rays which are harmful to his health. Robotic assistants are a very promising solution for these kind of interventions since they allow the protection of the practitioner while guaranteeing satisfactory accuracy. Such robotic systems working in the CT-scan ring already exist [2–4] and clinical trials have been performed yet. Nevertheless, these systems are not well suitable for all kind of percutaneous procedures, particularly for abdominal interventions in which the breathing of the patient has a great influence. In order to design a new robotic system, a list of the very severe medical requirements for these kind of procedures is presented. Only some of the most important constraints are given here since the reader will find further details in the literature [4, 5]. We point out that the nature of the working environment (X-rays) will add several constraints on the design of the robotic system.

Required Mobility of the Mechanism. To mimic a radiologist's dexterity, six degrees of freedom are theoretically required to hold and insert the needle. But from a practical point of view, the positioning and orientation of the needle can be dissociated from the insertion itself. The positioning and orientation will be achieved by the robotic device described in this paper. The required mobility thus corresponds to three degrees for positioning the entry point and two additional degrees for orienting the line supporting the needle axis (no self rotation). The insertion task will be achieved by a tool mounted as an end-effector on the robotic device, consequently giving more safety for the insertion itself. The description of this specific tool is beyond the scope of this document.

Dimensions of the CT-scan Gantry. A CT-scan imaging device looks like a bulky horizontal-axis ring of 700 mm in diameter. The patient is placed on a translating table that moves through the ring, leaving only a small space available for

special instruments. This is mainly due to the fact that most CT-scans are not designed for medical interventions. The typical free space for the radiologist is thus a 200 mm radius half-sphere centered at the entry point on the skin.

CT Image Plane. Computed tomography works by acquiring numerous X-rays projections of the patient's inner space, which is often called a CT-plane. This plane has a few millimeters width (10 to 30 mm) and vertically slices the patient body. As X-rays are very disrupted by metal and electrical devices, these materials must be avoided in the CT-plane. Since the mechanism has to hold the needle while the imaging device is acquiring a slice of the patient body, we must design our robot so that no metal parts cross the CT-plane.

Patient Safety, Exerted Forces and Accuracy. Safety and sterilization are critical requirements. Briefly, we can say that our system has to be attached to the patient body to avoid the breathing issue. It means that the robot is placed inside the CT ring and that it must be small enough to fit in the 200 mm half sphere. Furthermore, the robot must remain motionless in case of a failure in order to avoid an undesirable motion or bending of the needle. In [6] and our own experiments [7], we found that a maximum force of 20 N has to be applied on the needle during an insertion. This is a challenging constraint: in the same time the practitioner wants to have a precision of at least 1 mm. So, the accuracy and the rigidity of the system are other critical requirements.

Choice of the Structure. The design constraints we presented above limit the choice among the existing known mechanisms. Parallel structures are known mechanisms that are very well suited for absolute positioning accuracy and rigidity.

The paper is organized as follows. In the first section the robot is described using a local product of exponential representation and the closed-chain model is given. In the second section we calculate the forward and inverse kinematic models. Finally, in the last section we give simulation results (notably the workspace representation) and present the prototype built from our study.

DESCRIPTION OF THE MECHANISM

Our design is inspired by the work of Hunt [8] on the geometry of mechanisms. Tsai [9] proposes a methodology for creating and classifying mechanisms. According to this classification, the system we designed is made of one 6-bar linkage associated to a 4-bar linkage joined together by a common platform.

The structure has three legs, *i.e.* three serial chains joining the base to the platform. Let a reference frame i be denoted as $\mathcal{F}_i$, its origin as O_i and vectors typed in bold face. A frame $\mathcal{F}_0 = (O_0, \mathbf{x_0}, \mathbf{y_0}, \mathbf{z_0})$ is associated to the base of the robot and a frame $\mathcal{F}_f = (O_f, \mathbf{x_f}, \mathbf{y_f}, \mathbf{z_f})$ is associated to the platform (see Fig. 1). The first two opposite legs of the robot are symmetrical chains and form the planar 6-bar linkage. This linkage aims at constraining three degrees of freedom in its plane (Fig. 1(a)). They are namely the position of the point O_f and the orientation of the line (Δ_2) in the 6-bar linkage plane. The three controlled parameters associated to this 6-bar linkage are the variable lengths l_1, l_2 and the angle α.

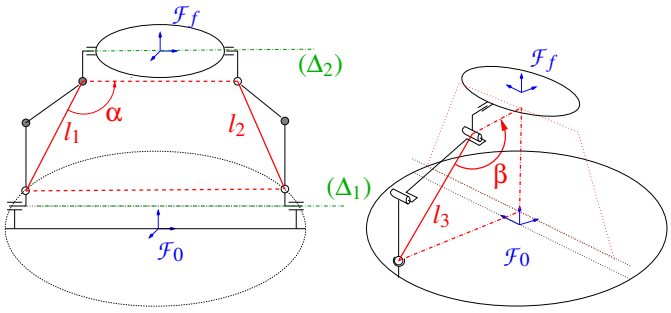

(a) THE 6-BAR LINKAGE (l_1,l_2,α), legs 1 and 2.

(b) THE 4-BAR LINKAGE (l_3,β), leg 3.

Figure 1. SIMPLIFIED REPRESENTATION

Once these two legs are positioned, two degrees of freedom still have to be defined using the third leg : the first one is the position of the origin O_f on a circle contained in a plane normal to the line (Δ_1). The second corresponds to the orientation of vector $\mathbf{z_f}$ about the line (Δ_2). The former is obtained by a rotation of the planar 6-bar linkage about the line (Δ_1) passing through the base (Fig. 1(a)). The latter corresponds to a platform rotation about the line (Δ_2). Finally, the last leg can be viewed as a 4-bar linkage with the variable length l_3 and angle β (Fig. 1(b)).

Both for practical and modeling reasons, the presented structure (see Fig. 2) is built only from revolute joints.

Modeling Formalism

Let us first introduce the mathematical notations we use for the modeling.

For any $i, j \in \mathbb{N}$, let c_i, s_i, t_i, $c_{i,j}$ and $s_{i,j}$ be $\cos(\theta_i)$, $\sin(\theta_i)$, $\tan(\frac{\theta_i}{2})$, $\cos(\theta_i + \theta_j)$ and $\sin(\theta_i + \theta_j)$. The coordinates of a vector $\mathbf{AB}$, expressed in $\mathcal{F}_i$ are denoted as ${}^iAB$. Its components are ${}^iAB_{[x]}$, ${}^iAB_{[y]}$, ${}^iAB_{[z]}$. The Euclidean norm of vector $\mathbf{AB}$ is $\|\mathbf{AB}\|$. The translation part of a homogeneous matrix ${}^{i-1}T_i$ is the vector ${}^{i-1}t = \mathrm{Trn}({}^{i-1}T_i)$ where $\mathrm{Trn}()$ is an application from $SE(3)$ to $\mathbb{R}^3$.

The modified Denavit-Hartenberg (DH) parameterization

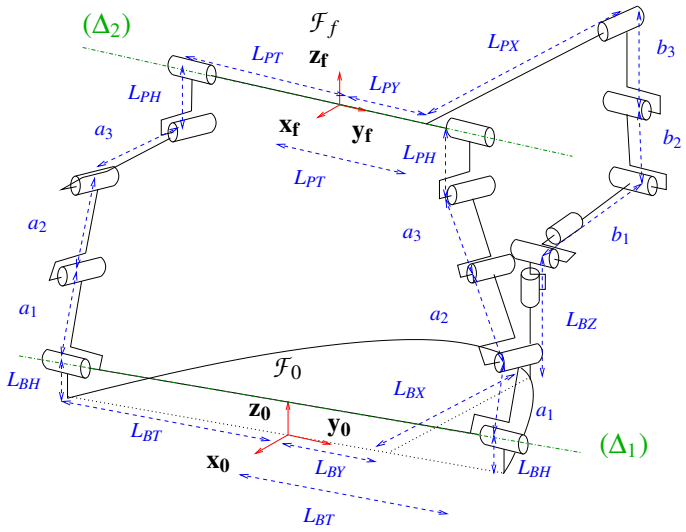

Figure 2. FUNCTIONAL SCHEMATIC OF THE ROBOT

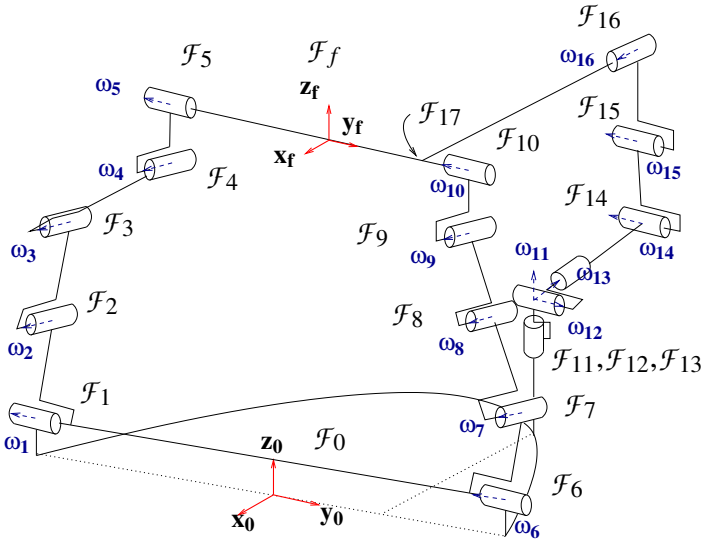

Figure 3. KINEMATIC MODEL OF THE ROBOT

[10] is undoubtly the most common way to describe serial robots in order to model them. An interesting alternative to the DH description is given by the product of exponential (POE) [11, 12]. This formalism has a comprehensive geometric interpretation and is easy to use both in the case of serial and parallel robots. To model a serial chain of a robot, we use the local product of exponentials (LPOE) as described in [13]. We briefly recall here the principle of this modeling.

We consider a serial mechanism for which the $i-$th joint connects two adjacent links. The frames $\mathcal{F}_{i-1}$ and $\mathcal{F}_i$ are associated to these successive links. The rigid transformation describing the pose of $\mathcal{F}_i$ relative to $\mathcal{F}_{i-1}$ is given by the LPOE transformation:

$$^{i-1}T_i(\theta_i) = {}^{i-1}T_i[\text{ext}]\, e^{\widehat{\xi}_i\theta_i} \tag{1}$$

where $^{i-1}T_i[\text{ext}] \in SE(3)$ is the initial fully extended configuration of frame $\mathcal{F}_i$ expressed in $\mathcal{F}_{i-1}$ when the parameter θ_i is 0:

$$^{i-1}T_i[\text{ext}] = \begin{bmatrix} ^{i-1}R_i & ^{i-1}O_{i-1}O_i \\ 0 & 1 \end{bmatrix}, \tag{2}$$

and $\widehat{\xi}_i$ is a twist associated with the $i-th$ joint. A twist is a compact representation of an element of $se(3)$ defined thanks to the instantaneous rotation axis $\omega_\mathbf{i}$, and the instantaneous translation velocity $\mathbf{v}$. This twist can be mapped to $SE(3)$ through an exponential map [11, 13]. To simplify calculations we consider that rotation matrices at initial configuration are identities: $^{i-1}R_i = I$. The position θ_i of the $i-th$ joint is refered to as q_i for the actuated joints and as p_i for the passive joints. The $i-th$ joint rotation axis $\omega_\mathbf{i}$ is oriented as defined on Fig. 3.

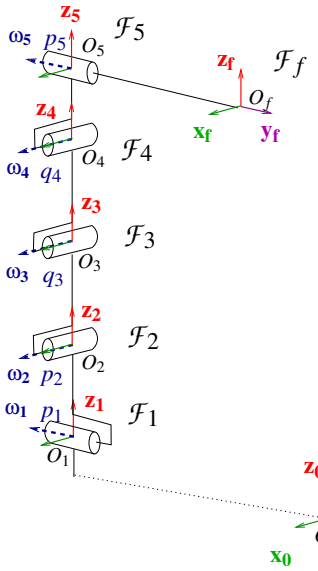

Figure 4. INITIAL CONFIGURATION OF THE FIRST LEG

The legs are considered independently and one can write their fully extended initial configuration joining frame $\mathcal{F}_0$ to $\mathcal{F}_f$. An example of the full extended configuration of leg one is shown on Fig. 4. The initial configuration of the three legs are defined by the tables 1, 2 and 3.

On each line of these tables, one can read the $\mathbb{R}^6$ vector of the twist coordinates of $\widehat{\xi}_i$. By applying the exponential map from $se(3)$ to $SE(3)$ it is possible to obtain the elementary homogeneous transformations. The composition of these matrices gives the forward kinematic models of the three legs which will

Table 1. INITIAL CONFIGURATION OF THE FIRST LEG.

Axis ${}^0\omega_i$	Joint i center position : ${}^0O_{i-1}O_i$	Joint i parameter θ_i
${}^0\omega_1 = \begin{bmatrix}0 & -1 & 0\end{bmatrix}^T$	${}^0O_0O_1 = \begin{bmatrix}0 & -L_{BT} & L_{BH}\end{bmatrix}^T$	p_1
${}^0\omega_2 = \begin{bmatrix}1 & 0 & 0\end{bmatrix}^T$	${}^1O_1O_2 = \begin{bmatrix}0 & 0 & a_1\end{bmatrix}^T$	p_2
${}^0\omega_3 = \begin{bmatrix}1 & 0 & 0\end{bmatrix}^T$	${}^2O_2O_3 = \begin{bmatrix}0 & 0 & a_2\end{bmatrix}^T$	q_3
${}^0\omega_4 = \begin{bmatrix}1 & 0 & 0\end{bmatrix}^T$	${}^3O_3O_4 = \begin{bmatrix}0 & 0 & a_3\end{bmatrix}^T$	q_4
${}^0\omega_5 = \begin{bmatrix}0 & -1 & 0\end{bmatrix}^T$	${}^4O_4O_5 = \begin{bmatrix}0 & 0 & L_{PH}\end{bmatrix}^T$	p_5
	${}^5O_5O_f = \begin{bmatrix}0 & L_{PT} & 0\end{bmatrix}^T$	

Table 2. INITIAL CONFIGURATION OF THE SECOND LEG.

Axis ${}^0\omega_i$	Joint i center position : ${}^0O_{i-1}O_i$	Joint i parameter θ_i
${}^0\omega_6 = \begin{bmatrix}0 & -1 & 0\end{bmatrix}^T$	${}^0O_0O_6 = \begin{bmatrix}0 & L_{BT} & L_{BH}\end{bmatrix}^T$	p_6
${}^0\omega_7 = \begin{bmatrix}1 & 0 & 0\end{bmatrix}^T$	${}^0O_6O_7 = \begin{bmatrix}0 & 0 & a_1\end{bmatrix}^T$	p_7
${}^0\omega_8 = \begin{bmatrix}1 & 0 & 0\end{bmatrix}^T$	${}^0O_7O_8 = \begin{bmatrix}0 & 0 & a_2\end{bmatrix}^T$	q_8
${}^0\omega_9 = \begin{bmatrix}1 & 0 & 0\end{bmatrix}^T$	${}^0O_8O_9 = \begin{bmatrix}0 & 0 & a_3\end{bmatrix}^T$	p_9
${}^0\omega_{10} = \begin{bmatrix}0 & -1 & 0\end{bmatrix}^T$	${}^0O_9O_{10} = \begin{bmatrix}0 & 0 & L_{PH}\end{bmatrix}^T$	p_{10}
	${}^0O_{10}O_f = \begin{bmatrix}0 & -L_{PT} & 0\end{bmatrix}^T$	

Table 3. INITIAL CONFIGURATION OF THE THIRD LEG.

Axis ${}^0\omega_i$	Joint i center position : ${}^0O_{i-1}O_i$	Joint i parameter θ_i
${}^0\omega_{11} = \begin{bmatrix}0 & 0 & 1\end{bmatrix}^T$	${}^0O_0O_{11} = \begin{bmatrix}-L_{BX} & L_{BY} & L_{BZ}\end{bmatrix}^T$	p_{11}
${}^0\omega_{12} = \begin{bmatrix}0 & 1 & 0\end{bmatrix}^T$	${}^0O_{11}O_{12} = \begin{bmatrix}0 & 0 & 0\end{bmatrix}^T$	p_{12}
${}^0\omega_{13} = \begin{bmatrix}0 & 0 & 1\end{bmatrix}^T$	${}^0O_{12}O_{13} = \begin{bmatrix}0 & 0 & 0\end{bmatrix}^T$	p_{13}
${}^0\omega_{14} = \begin{bmatrix}0 & -1 & 0\end{bmatrix}^T$	${}^0O_{13}O_{14} = \begin{bmatrix}0 & 0 & b_1\end{bmatrix}^T$	q_{14}
${}^0\omega_{15} = \begin{bmatrix}0 & -1 & 0\end{bmatrix}^T$	${}^0O_{14}O_{15} = \begin{bmatrix}0 & 0 & b_2\end{bmatrix}^T$	q_{15}
${}^0\omega_{16} = \begin{bmatrix}1 & 0 & 0\end{bmatrix}^T$	${}^0O_{15}O_{16} = \begin{bmatrix}0 & 0 & b_3\end{bmatrix}^T$	p_{16}
	${}^0O_{16}O_f = \begin{bmatrix}L_{PX} & -L_{PY} & 0\end{bmatrix}^T$	

be denoted g_{0f_k} ($k \in \{1,2,3\}$).

KINEMATIC MODELING

The platform configuration should be expressed by five parameters corresponding to the number of degrees of freedom of the platform. A possible solution is to consider: i) the platform origin O_f with coordinates: $[{}^0O_0O_{f\ [x]}\ {}^0O_0O_{f\ [y]}\ {}^0O_0O_{f\ [z]}]^T$ in $\mathcal{F}_0$; ii) the normal unit vector attached to the platform and pointing upward, with coordinates $[{}^0z_{f\ [x]}\ {}^0z_{f\ [y]}\ {}^0z_{f\ [z]}]^T$ in $\mathcal{F}_0$ (only two degrees of freedom since the norm of the vector equals one).

Inverse Kinematics

Angle Between the Base and the First Closed Chain. Let us rewrite the position of point O_f in $\mathcal{F}_1$. We know that the first and second leg lie in the same plane, so that only one angle p_1 can determine ${}^0O_0O_{f\ [x]}$ and ${}^0O_0O_{f\ [z]}$, for a given distance between O_1 and O_f:

$$ {}^0O_1O_{f\ [x]} = -||\mathbf{O_1O_f}||s_1, \tag{3}$$

$$ {}^0O_1O_{f\ [z]} = ||\mathbf{O_1O_f}||c_1. \tag{4}$$

From Fig. 3, ${}^0O_1O_{f\ [x]} = {}^0O_0O_{f\ [x]}$ and ${}^0O_1O_{f\ [z]} = {}^0O_0O_{f\ [z]} - L_{BH}$. Finally:

$$ p_1 = \arctan2(-{}^0O_0O_{f\ [x]},\ {}^0O_0O_{f\ [z]} - L_{BH}). \tag{5}$$

First Leg. The first leg forward kinematics can be projected in the (O_1, O_6, O_f) plane by premultiplying g_{0f_l} by ${}^1T_0$. Hence the vector $\mathbf{O_5O_f}$ in $\mathcal{F}_1$ should have a null coordinate ${}^1O_5O_{f\ [x]}$:

$$ \mathbf{O_5O_f} = \mathbf{O_0O_f} - \mathbf{O_0O_5}. \tag{6}$$

This will be useful to obtain the angles p_2, q_3 and q_4. The result is obtained by taking the translation part of the following homogeneous matrix:

$$ {}^1O_5O_f = \mathrm{Trn}\left({}^1T_0 g_{0f_l}\left(I - {}^fT_5\right)\right). \tag{7}$$

As we have the constraint that $\mathbf{z_f}$ is orthogonal to $\mathbf{O_5O_f}$, we obtain:

$$ \left({}^1O_5O_f\right)^T {}^1z_f = L_{PT}\left({}^1z_{f\,[y]}c_{2,3,4} + ({}^1z_{f\,[z]}c_1 - {}^1z_{f\,[x]}s_1)s_{2,3,4}\right) = 0. \tag{8}$$

Then we proceed to the substitution $c_{2,3,4} = \varepsilon\sqrt{1 - {s_{2,3,4}}^2}$ with $\varepsilon \in \{-1,1\}$ in the previous equation. This substitution introduces a new supplementary solution that has mathematically to be considered. Once solved for $s_{2,3,4}$, we have:

$$ s_{2,3,4} = \frac{\varepsilon\ {}^1z_{f\,[y]}}{\sqrt{{}^1z_{f\,[y]}^2 + {}^1z_{f\,[x]}^2{s_1}^2 - 2\,{}^1z_{f\,[x]}\,{}^1z_{f\,[z]}s_1c_1 + {}^1z_{f\,[z]}^2{c_1}^2}} \tag{9}$$

The denominator of $s_{2,3,4}$ is never null since it is a sum of quadratic terms and no singularity may appear in this equation.

The ε indeterminate represents a symmetric orientation of the platform relative to the base frame with respect to the (O_f, $\mathbf{x_0}$, $\mathbf{z_0}$) plane. Numerically, we find that $\varepsilon = -1$ corresponds to the correct orientation.

Because we only know the sine of $\Sigma_{2,3,4} = p_2 + q_3 + q_4$, again two solutions are possible. To solve this, we impose a mechanical constraint: we suppose that the platform vector $\mathbf{z_f}$ makes a maximum angle of $\pm\frac{\pi}{2}$ with the base vector $\mathbf{z_0}$ about $\mathbf{x_0}$. The angle $\arcsin(s_{2,3,4})$ is then entirely defined in $]-\frac{\pi}{2},\frac{\pi}{2}[$.

Now we solve for the whole kinematic chain. Let's compute $\mathbf{O_1O_4}$ by two different ways. First by using the first leg:

$$\begin{aligned} {}^1O_1O_{4|\text{Leg 1}} &= \text{Trn}\left({}^1T_2\,{}^2T_3\,{}^3T_4\right) \\ &= \begin{bmatrix} 0 \\ -a_2s_2 - a_3s_{2,3} \\ a_1 + a_2c_2 + a_3c_{2,3,4} \end{bmatrix}. \end{aligned} \tag{10}$$

Then going by the platform:

$${}^1O_1O_{4|\text{Pl}} = \begin{bmatrix} {}^0O_0O_{f\,[x]}c_1 + ({}^0O_0O_{f\,[z]} - L_{BH})s_1 \\ {}^0O_0O_{f\,[y]} + L_{BT} - L_{PT}c_{2,3,4} + L_{PH}s_{2,3,4} \\ ({}^0O_0O_{f\,[z]} - L_{BH})c_1 - {}^0O_0O_{f\,[x]}s_1 - L_{PT}s_{2,3,4} - L_{PH}c_{2,3,4} \end{bmatrix}. \tag{11}$$

If we sum the square of the Y and Z coordinates in Eqns. (10) and (11), we obtain:

$$\left({}^1O_1O_{4|\text{Pl }[y]}\right)^2 + \left({}^1O_1O_{4|\text{Pl }[z]}\right)^2 = {a_2}^2 + 2a_2a_3c_3 + a_3^2, \tag{12}$$

that allows to compute:

$$q_3 = \pm\arccos\left(\frac{\left({}^1O_1O_{4|\text{Pl }[y]}\right)^2 + \left({}^1O_1O_{4|\text{Pl }[z]}\right)^2 - a_2^2 - a_3^2}{2a_2a_3}\right). \tag{13}$$

Among the two solutions, we choose $q_3 \leq 0$ for mechanical reasons. Then we obtain p_2 by the substitution: $s_2 = \frac{2t_2}{1+t_2^2}$ and $c_2 = \frac{1-{t_2}^2}{1+{t_2}^2}$ in Eqn. (10). After this substitution, we solve for t_2 and have:

$$t_2 = \frac{a_2 + a_3c_3 \pm \sqrt{a_2^2 + 2a_2a_3c_3 + a_3^2 - \left({}^1O_1O_{4|\text{Pl }[y]}\right)^2}}{a_3s_3 - {}^1O_1O_{4|\text{Pl }[y]}}. \tag{14}$$

A singularity is shown when $a_3s_3 = {}^1O_1O_{4|\text{Pl }[y]}$. This means that O_1 and O_4 are superimposed, which should not happen in reality. A final step gives:

$$p_2 = 2\arctan(t_2), \tag{15}$$

and finally:

$$q_4 = \Sigma_{2,3,4} - p_2 - q_3. \tag{16}$$

Second Leg. We use the same type of resolution for the second leg. We now consider vector $\mathbf{O_{10}O_f}$ in frame $\mathcal{F}_6$. The orthogonal constraint gives the following equation:

$$\left({}^6O_{10}O_f\right)^T {}^6z_f = L_{PT}\left({}^6z_{f\,[y]}c_{7,8,9} + ({}^6z_{f\,[z]}c_6 - {}^6z_{f\,[x]}s_6)s_{7,8,9}\right) = 0. \tag{17}$$

Then we solve for $s_{7,8,9}$:

$$s_{7,8,9} = \frac{\varepsilon'\,{}^6z_{f\,[y]}}{\sqrt{{}^6z_{f\,[y]}^2 + {}^6z_{f\,[x]}^2 s_6^2 - 2s_6c_6{}^6z_{f\,[x]}^2\,{}^6z_{f\,[z]}^2 + {}^6z_{f\,[z]}^2 c_6{}^2}}. \tag{18}$$

This gives another supplementary solution for $s_{7,8,9}$. As before, $\varepsilon' = -1$ and again two solutions exist for $\Sigma_{7,8,9} = p_7 + q_8 + p_9$. This is solved because $\Sigma_{7,8,9} = \arcsin(s_{7,8,9}) \in]-\frac{\pi}{2},\frac{\pi}{2}[$ for practical reasons.

The kinematic chain is solved by computing ${}^6O_6O_{9|\text{Pl}}$ and ${}^6O_6O_{9|\text{Leg 2}}$ as before. After equaling the squared sum of the Y and Z coordinates :

$$\left({}^6O_6O_{9|\text{Pl }[y]}\right)^2 + \left({}^6O_6O_{9|\text{Pl }[z]}\right)^2 = {a_2}^2 + 2a_2a_3c_8 + {a_3}^2, \tag{19}$$

and so we have:

$$q_8 = \pm\arccos\left(\frac{\left({}^6O_6O_{9|\text{Pl }[y]}\right)^2 + \left({}^6O_6O_{9|\text{Pl }[z]}\right)^2 - {a_2}^2 - {a_3}^2}{2a_2a_3}\right). \tag{20}$$

And here we choose $q_8 \geq 0$ for mechanical reasons. As before, p_7 is obtained by the substitution $s_7 = \frac{2t_7}{1+t_7^2}$:

$$t_7 = \frac{a_2 + a_3c_8 \pm \sqrt{{a_2}^2 + 2a_2a_3c_8 + {a_3}^2 - \left({}^6O_6O_{9|\text{Pl }[y]}\right)^2}}{a_3s_6 - {}^6O_6O_{9|\text{Pl }[y]}}. \tag{21}$$

We find a singularity in t_7 with the same meaning as for leg one. Then :

$$p_7 = 2\arctan(t_7), \tag{22}$$

and finally:

$$p_9 = \Sigma_{7,8,9} - p_7 - q_8. \tag{23}$$

Platform Angle. For p_5 (or p_{10}), which is the last angle that has to be found, we compute ${}^0z_f$ by using the first leg forward kinematics. This gives:

$${}^0z_f = \begin{bmatrix} -c_1s_5 - s_1c_5 \\ -c_5s_{2,3,4} \\ -s_1s_5 + c_1c_5c_{2,3,4} \end{bmatrix}. \tag{24}$$

As this vector is known, we compute c_5 and s_5 that define completely the angle:

$$p_5 = \arctan 2\left(-c_1{}^0z_{f\,[x]} - s_1{}^0z_{f\,[z]}, \frac{c_1{}^0z_{f\,[z]} - s_1{}^0z_{f\,[x]}}{c_{2,3,4}}\right). \tag{25}$$

A singularity is possible if $c_{2,3,4} = 0$. This is the case when $\mathbf{z_f}$ is collinear with $\mathbf{y_0}$, what should not happen.

Third Leg. Once we have solved the first 6-bar linkage, we can define the platform orientation thanks to $\mathbf{x_f}$, $\mathbf{y_f}$ and $\mathbf{z_f}$. The last leg has six degrees of freedom and can be solved by position/orientation considerations.

The first passive parameter to be found is p_{16}. It is the angle between the planes (O_f, $\mathbf{x_f}$, $\mathbf{z_f}$) and (O_{16}, $\mathbf{z_{16}}$, $\mathbf{y_{16}}$). This angle is also the angle between the Y component and Z component of ${}^fO_{13}O_{16}$. As :

$$ {}^fO_{13}O_{16} = {}^fR_0\,{}^0O_{13}O_f + {}^fO_fO_{16}, \tag{26} $$

we get:

$$ \begin{aligned} p_{16} = \arctan 2\big(((L_{BX} + {}^0O_0O_{f_{[x]}})s_1 - c_1)s_{2,3,4} + \\ (L_{BY} - {}^0O_0O_{f_{[y]}})c_{2,3,4} - L_{PY}, \\ {}^0z_{[x]}({}^0O_0O_{f_{[x]}} + L_{BX}) + {}^0z_{[y]}({}^0O_0O_{f_{[y]}} - L_{BY}) + \\ {}^0z_{[z]}({}^0O_0O_{f_{[z]}} - L_{BZ})\big). \end{aligned} \tag{27} $$

The last two parameters q_{14} and q_{15} are obtained by first computing the vector $\mathbf{O_{13}O_{15}}$ with the forward kinematics of the leg and then by computing it using frames $\mathcal{F}_0$, $\mathcal{F}_f$, and $\mathcal{F}_{16}$. This is similar to the previous calculus for legs one and two:

$$ {}^{15}O_{13}O_{15[x]} = -b_1 s_{14,15} + b_2 s_{15}, \tag{28} $$

$$ {}^{15}O_{13}O_{15[z]} = -b_1 c_{14,15} - b_2 c_{15}, \tag{29} $$

$$ \left({}^{15}O_{13}O_{15[x]}\right)^2 + \left({}^{15}O_{13}O_{15[z]}\right)^2 = {b_2}^2 + 2b_1b_2c_{14} + {b_1}^2. \tag{30} $$

Hence we have two solutions for q_{14}, but, because of mechanical design, q_{14} is always in $\in [0,\pi]$ and so:

$$ q_{14} = \arccos\left(\frac{\left({}^{15}O_{13}O_{15[x]}\right)^2 + \left({}^{15}O_{13}O_{15[z]}\right)^2 - {b_2}^2 - {b_1}^2}{2b_1b_2}\right). \tag{31} $$

Finally, we substitute t_{15} ($= \tan\frac{q_{15}}{2}$) in Eqns. (28) and (29). After computations and solving for t_{15}, we obtain:

$$ q_{15} = -2\arctan\left(\frac{b_1c_{14} + b_2 \pm \sqrt{b_1^2 + b_2^2 + 2b_1b_2c_{14} - \left({}^{15}O_{13}O_{15[x]}\right)^2}}{{}^{15}O_{13}O_{15[x]} - b_1s_{14}}\right), \tag{32} $$

which gives another singularity when $b_1 s_{14} = {}^{15}O_{13}O_{15[x]}$.

Forward Kinematics

First 6-bar Linkage. We study the first 6-bar linkage in $\mathcal{F}_1$. This linkage has three degrees of freedom in the plane (O_1, $\mathbf{z_1}$, $\mathbf{y_1}$): position and orientation. This linkage has three actuated joints q_3, q_4 and q_8. Hence we should be able to completely define its configuration.

When only p_2, q_3 and q_4 are given, a point on the first leg draws a circle about the line (Δ_1) due to the angle p_1. To remove this dependence, all the next computations are made in $\mathcal{F}_1$, so that the point ${}^1O_2$ becomes static.

Due to the mechanical design, O_9 also lies in the same plane (O_1, $\mathbf{z_1}$, $\mathbf{y_1}$), and p_3 does not change its position in $\mathcal{F}_1$. From Fig. (3), it is clear that only p_2 completely determines the position of O_9 in $\mathcal{F}_1$ since O_9 describes a circle centered at O_2.

We consider the radius of this circle to be a constant distance : $||\mathbf{O_2O_9}||$ which can be calculated thanks to the projection of $\mathbf{O_2O_9}$ in $\mathcal{F}_1$:

$$ {}^1O_2O_9 = \begin{bmatrix} 0 \\ 2L_{PT}c_{2,3,4} - a_2s_2 - a_3s_{2,3} \\ 2L_{PT}s_{2,3,4} + a_2c_2 + a_3c_{2,3} \end{bmatrix}. \tag{33} $$

Then:

$$ ||\mathbf{O_2O_9}||^2 = 4L_{PT}\left(L_{PT} + a_2s_{3,4} + a_3s_4\right) + a_2^2 + a_3^2 + 2a_2a_3c_3\,. \tag{34} $$

The second leg has the same property as the first leg, *i.e.* each point generates a circle about (Δ_1). If we suppose that q_8 is constant, the movement of O_9 in $\mathcal{F}_6$ is a circle centered at O_7 with a radius of $||\mathbf{O_7O_9}||$. As before:

$$ ||\mathbf{O_7O_9}||^2 = a_2^2 + a_3^2 + 2a_2a_3c_8. \tag{35} $$

Then we obtain the intersection between these two circles. Geometrically, this intersection is O_9 and its position is expressed in $\mathcal{F}_1$ by:

$$ ({}^1O_1O_{9[y]})^2 + ({}^1O_1O_{9[z]})^2 = ||\mathbf{O_2O_9}||^2, \tag{36} $$

$$ \left({}^1O_1O_{9[y]} - 2L_{BT}\right)^2 + ({}^1O_1O_{9[z]})^2 = ||\mathbf{O_7O_9}||^2. \tag{37} $$

We subtract Eqn. (37) from Eqn. (36) and solve for ${}^1O_1O_{9[y]}$ and ${}^1O_1O_{9[z]}$:

$$ {}^1O_1O_{9[y]} = \frac{L_{BT}^2 + ||\mathbf{O_2O_9}||^2 - ||\mathbf{O_7O_9}||^2}{4L_{BT}}, \tag{38} $$

$$ {}^1O_1O_{9[z]} = \pm\sqrt{||\mathbf{O_2O_9}||^2 - ({}^1O_1O_{9[y]})^2}. \tag{39} $$

Two symmetrical solutions are possible, but in reality, only ${}^1O_1O_{9[z]} > 0$ will be kept (platform above the base). As we know the position of O_9, we deduce the angle p_2 of the first leg from Eqn. (33) :

$$ \begin{aligned} {}^1O_1O_{9[y]} &= \underbrace{(-a_3s_3 + 2L_{PT}c_{3,4})}_{u_1}c_2 + \underbrace{(-a_2 - a_3c_3 - 2L_{PT}s_{3,4})}_{u_2}s_2, \\ {}^1O_1O_{9[z]} &= -u_2c_2 + u_1s_2. \end{aligned} \tag{40} $$

We finally deduce c_2 and s_2, which give p_2:

$$ p_2 = \arctan 2\left(\frac{u_1\,{}^1O_1O_{9[z]} + u_2\,{}^1O_1O_{9[y]}}{u_1^2 + u_2^2}, \frac{-u_2\,{}^1O_1O_{9[z]} + u_1\,{}^1O_1O_{9[z]}}{u_1^2 + u_2^2}\right). \tag{41} $$

With the same method, we obtain for p_9:

$$ \begin{aligned} {}^1O_1O_{9[y]} &= \underbrace{-a_3s_3}_{u_3}c_9 + \underbrace{(-a_2 - a_3c_3)}_{u_4}s_9 + 2L_{BT}, \\ {}^1O_1O_{9[z]} &= -u_4c_9 + u_3s_9 + 2L_{BT}. \end{aligned} \tag{42} $$

Once solved :

$$p_9 = \arctan 2\left(\frac{u_3{}^1O_1O_{9[z]} + u_4{}^1O_1O_{9[y]} - 2u_4L_{BT}}{u_3^2+u_4^2}, \frac{-u_4{}^1O_1O_{9[z]} + u_3{}^1O_1O_{9[y]} - 2u_3L_{BT}}{u_3^2+u_4^2}\right). \quad (43)$$

The last parameter to be found is p_4. Expressing the loop closure of the 6-bar linkage we have:

$$p_7 = p_2 + q_3 + q_4 - p_9 - q_8. \quad (44)$$

Second 4-bar linkage. When q_{14} and q_{15} are fixed, $\mathbf{O_{13}O_{17}}$ has a constant norm that can be identified as the length of the third leg (see Fig. 3). Hence O_{17} is positioned on a sphere centered at O_{13} with a radius of $||\mathbf{O_{13}O_{17}}||$. This norm is obtained and computed thanks to the forward kinematics of the third leg by :

$$^{13}O_{13}O_{17} = \mathrm{Trn}\left(^{13}T_{14}{}^{14}T_{15}{}^{15}T_{16}{}^{16}T_{17}\right), \quad (45)$$

$$= \begin{bmatrix} L_{PX}c_{14,15} - b_3s_{14,15} - b_2s_{14} \\ 0 \\ L_{PX}s_{14,15} + b_3c_{14,15} + b_2s_{14} + b_1 \end{bmatrix}. \quad (46)$$

On the other hand, the first 6-bar linkage is already fully solved, and we obtain the position of O_{17} by computing the forward kinematics of the first leg and by an appropriate proportional adjustment:

$$\mathbf{O_1O_{17}} = \frac{L_{BT}+L_{PY}}{L_{PT}}(\mathbf{O_1O_f} - \mathbf{O_1O_5}). \quad (47)$$

In $\mathcal{F}_1$:

$$^1O_1O_{17} = \begin{bmatrix} 0 \\ -a_2s_2 - a_3s_{2,3} - L_{PH}s_{2,3,4} + (L_{PT}+L_{PY})c_{2,3,4} \\ a_1 + a_2c_2 + a_3c_{2,3} + L_{PH}c_{2,3,4} + (L_{PT}+L_{PY})s_{2,3,4} \end{bmatrix}. \quad (48)$$

Because of the passive joint p_1, O_{17} draws a circle about (Δ_1). If we write $\mathcal{P}(O_{17})$ the orthogonal projection of O_{17} on (Δ_1), then O_{17} lies on the circle centered at $\mathcal{P}(O_{17})$ with radius $||\mathcal{P}(\mathbf{O_{17}})\mathbf{O_{17}}||$. The first problem is to find the position of $\mathcal{P}(O_{17})$ in $\mathcal{F}_O$. We know that $\mathcal{P}(O_{17})$ has the same Y coordinate as $^0O_{17}$, additionally its X and Z coordinates are those of O_1 in $\mathcal{F}_0$, so:

$$^0\mathcal{P}(O_{17}) = \begin{bmatrix} 0 \\ -a_3s_{2,3} - L_{PH}s_{2,3,4} + (L_{PT}+L_{PY})c_{2,3,4} - L_{BT} \\ L_{BH} \end{bmatrix}. \quad (49)$$

If we define a new coordinate frame $\mathcal{F}_{\mathcal{P}(O_{17})} = (\mathcal{P}(O_{17}), \mathbf{x_0}, \mathbf{y_0}, \mathbf{z_0})$, we can express all the unknown terms in this frame coordinate, attached to $\mathcal{P}(O_{17})$ with the same orientation as $\mathcal{F}_0$. The equation of the circle becomes:

$$||\mathcal{P}(\mathbf{O_{17}})\mathbf{O_{17}}||^2 = (^0O_0O_{17[x]})^2 + (^0O_0O_{17[z]})^2, \quad (50)$$

and the sphere of the third leg becomes:

$$||\mathbf{O_{13}O_{17}}||^2 = (^0O_0O_{17[x]} + L_{BX})^2 + (^0O_0O_{17[z]} - L_{BZ} + L_{BH})^2 + (L_{BY} - {}^0O_0O_{17[y]})^2. \quad (51)$$

Then Eqns. (50) and (51) lead to an equation of the form: $a(^0O_0O_{17[z]})^2 + b(^0O_0O_{17[z]}) + c = 0$, with $a,\ b,\ c \in \mathbb{R}$. Thus we have two solutions for $^0O_0O_{17[z]}$ and therefore two solutions for $^0O_0O_{17[x]}$. Once solved, we get the position of O_{17} in $\mathcal{F}_0$. Finally:

$$p_1 = \arctan 2(^0O_0O_{17[x]}, {}^0O_0O_{17[z]} - L_{BH}). \quad (52)$$

Hence the position of O_f in $\mathcal{F}_O$ is determined.

The Platform Vector $\mathbf{z_f}$. To obtain the full configuration of the platform, we do need to find the $\mathbf{z_f}$ vector. This is equivalent to find the position of O_{16} in $\mathcal{F}_O$ if we remember that :

$$\mathbf{z_f} = \frac{\mathbf{O_fO_{17}} \times \mathbf{O_{17}O_{16}}}{||\mathbf{O_fO_{17}} \times \mathbf{O_{17}O_{16}}||}. \quad (53)$$

This problem is similar to the previous one and the way to solve it is almost the same: we look for the intersection between a circle generated by O_{16} centered at O_{17} about the axis $\mathbf{y_f}$ with a radius of $||\mathbf{O_{17}O_{16}}||$ and a sphere generated by O_{16} centered at O_{13} with a radius of $||\mathbf{O_{13}O_{16}}||$.

For brevity the solution of this problem is not described here but it leads to at least two results that are mechanically possible. This is a common problem in forward kinematics of parallel structures, and we cannot *a priori* solve the issue by verifying each choice and comparing the pose. However, the two solutions are easily distinguished as one gives a posture where the third leg lies inside the working space and the other, symmetrically, gives a posture outside the working space.

Approximated Jacobian

The computation of the Jacobian matrix J of the system is of great importance both for design and control purposes. Indeed, for a given operational force F, the torque on each actuated joint can be computed using the classical equation:

$$\tau = J^T F. \quad (54)$$

This is very useful for the optimization of the length parameters with respect to the rigidity. Additionally, the condition number (the smallest singular value of J divided by the largest one) provides a good measure of the manipulability of the robot at an operating point. In our particular case, we cannot easily derive the equation of neither the inverse nor the forward instantaneous kinematic model. We thus had to compute the approximation of the Jacobian matrix, based on the numerical derivative of the forward kinematics solution.

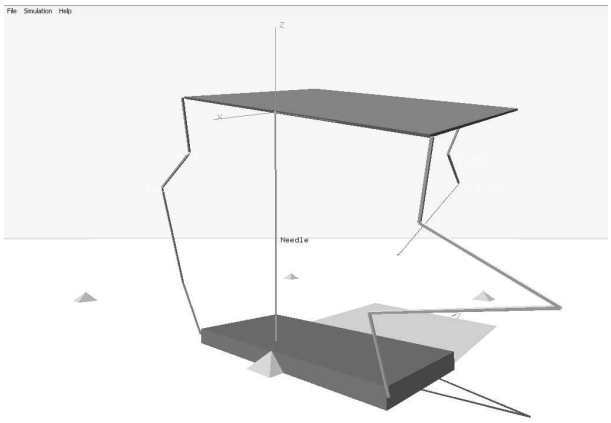

Figure 5. NUMERICAL SIMULATION USING A DYNAMIC ENGINE

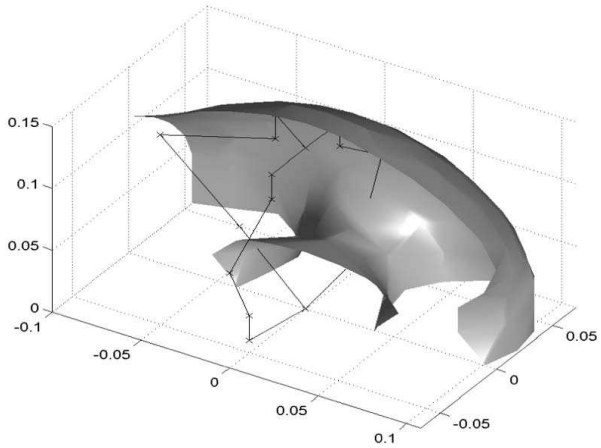

Figure 6. SIMPLIFIED WORKSPACE OF THE ROBOT

RESULTS

The inverse kinematic inputs ${}^0O_0O_f$ and ${}^0z_f$ can be transformed to spherical-like coordinates, very convenient for representing the configuration of the platform :

- the entry point: ${}^0O_0E = \left[E_{[x]}\ E_{[y]}\ E_{[z]}\right]^T$;
- two rotation angles about this entry point: rotation about the axis $\mathbf{x_0}$ and $\mathbf{y_0}$ (angles ϕ and θ);
- a constant platform altitude: ρ.

The position of the entry point and ρ are redundant information. So we consider ρ to be a constant that should not change over time (it is the altitude relative to the entry point). Once given this additional constraint, we can compute the previous set of parameters by the transformation:

$$ {}^0z_f = \begin{bmatrix} \cos(\theta)\sin(\phi) \\ -\sin(\theta) \\ \cos(\theta)\cos(\phi) \end{bmatrix}, \quad {}^0O_0O_f = {}^0O_0E + \rho \times {}^0z_f. \tag{55} $$

Numerical Simulation Using a Dynamic Engine

In order to verify the possible motions of the mechanism, we used a numerical dynamic engine in C++ (Open Dynamic Engine [14]) to build a virtual mechanism with the same geometry as our robot (Fig. 5).

We implemented the inverse and forward kinematics to verify the positioning and orientation part of our model. For a given load applied on the platform, the simulations confirm that the mechanism can be kept in equilibrium by acting on the five actuated joints. Future work will include trajectory planning and self-collision checking.

Reachable Workspace

This robot has five degrees of freedom, and therefore its reachable workspace is difficult to plot. The workspace is thus defined as the reachable 3D space of the platform origin O_f for a given configuration of ${}^0z_f$. We present here only a particular configuration for ${}^0z_f$: $\theta = 0$, $\phi = 0$. A Matlab plot of the half wrapping surface of the workspace is given on Fig. 6. As shown, the workspace is almost spherical. Again, the possible self collisions in the physical prototype will have to be taken into account in the future for a more precise analysis.

Physical Prototype.

CT-Bot is the name given to the physical prototype of which building is on-going. In this section we survey the main steps of the prototype design with some details concerning the mechanical structure and the drive system. Figure 7 depicts the general layout of the patient and the robotic device before he enters the CT-scan ring.

The design process has been conducted with an extensive usage of CAD system. Starting from the structural description of the robot (mechanism topology, number of bodies, type of joints) we modeled the robot to define its kinematics. At this stage, the structure of the robot consists of sets of lines and points that represent its skeleton.

Then the different components were designed with a direct relationship with the robot skeleton. This top-down design approach takes advantage of the initial parameterization and enables to change characteristic dimensions on the structure without re-designing the parts.

Mechanical Structure of the CT-Bot Prototype. A robot base support is attached with straps on the patient body. An adequate interface between the robot base and the skin of the patient is under development. The robot itself is then oriented and fixed on the base support. This feature allows to choose the best initial configuration according to the intervention objective.

Figure 7. GENERAL LAYOUT

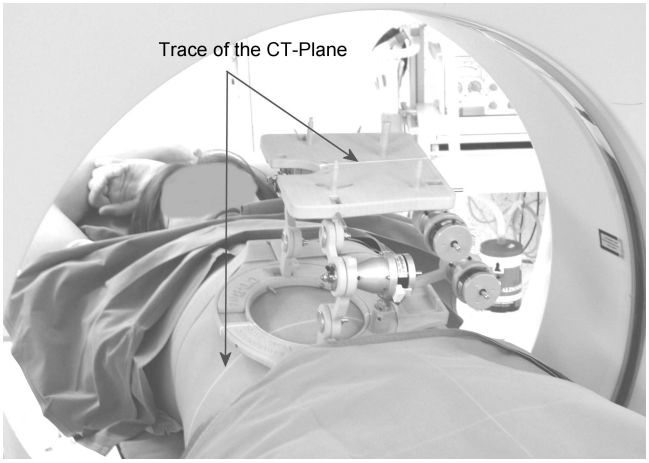

Figure 8. CT-BOT IN THE CT-SCAN

In the mechanical design of the links we used bearings to limit friction and backlash. A special care was taken to increase structural stiffness of the system.

Figure 8 (physical prototype) and Fig. 9 (the robot CAD model) illustrate how we placed the third leg of the robot at a certain distance away from the (O_0, $\mathbf{x_0}$, $\mathbf{y_0}$) plane to limit the number of non-plastic parts in the CT-plane. Similarly we oriented actuation units of the third leg away from the CT-plane.

Drive System. Each actuation unit comprises a gear housing specifically designed for this application, an Harmonic Drive reduction gearing, an ultrasonic motor and an incremental encoder. Ultrasonic motors have several advantages over other type of actuators including :

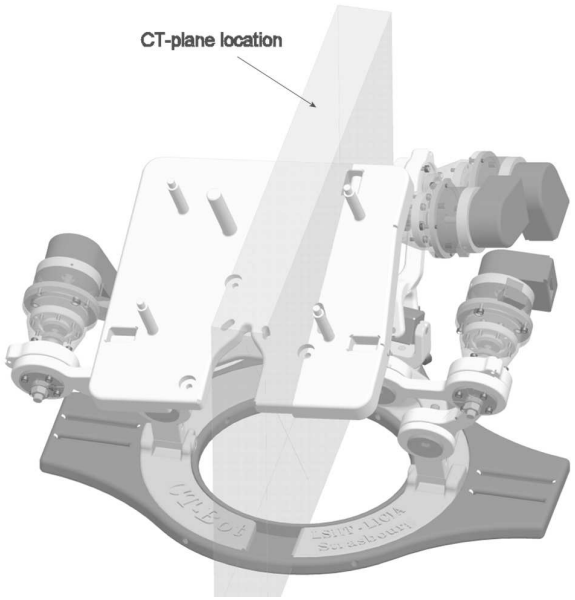

Figure 9. CT-BOT CAD-MODEL

- a good torque to weight ratio ;
- a low rotational speed ;
- a high holding torque when not powered.

These features are important for our application from the point of view of the effort to be exerted by the robot and the required safety for this medical device. In case of a control failure, the robot holding the needle will remain motionless.

The resulting actuation unit has an outer size included in a cylinder of 75 mm in length and 50 mm in diameter.

Manufacturing. Most of the parts composing the robot have been obtained through rapid prototyping with a laser sintering system. This enables to move directly from CAD files to functional plastic parts in a fraction of the time required for traditional machining and tooling processes. The material employed is glass-filled polyamide powder to comply with the CT-Scan imaging requirements.

So far, the following elements have been achieved on the prototype :

- construction of the different robot components ;
- mechanical assembly of the robot.

The forthcoming stages concerning the physical prototype include the resolution of sterilization-related issues. These constraints were present from the beginning in the design process and practical solutions are to be implemented to pass medical approval. Some preliminary orientations have already been chosen.

Another important subject is the needle insertion tool to be mounted as an end-effector on the platform. This system comprises force sensor and will be crucial for task execution and will be detailled in future communication.

CONCLUSION

A new five-degree-of-freedom parallel manipulator has been presented in order to help practitioners in percutaneous interventions realized under X-rays imaging devices. These medical procedures imply many strong constraints on the robotic assistant such as transparency to X-rays, compactness, stiffness and safety.

The modeling of the mechanism has been conducted using the local product of exponentials formalism. Numerical simulations on a wire-frame system enabled to check the main limits of the operational workspace. The results obtained from inverse kinematic analysis were input data to the design process. Starting from topological and dimensional description of the structure, a fully parametric CAD model of the robot has been built. This model helped to iteratively improve the design and take into account the technical limitations (actual geometry of the parts, mechanical stops).

As a current result, a physical prototype has been built. Remaining tasks include cabling, electrical connection and construction of the insertion tool to be mounted as an end-effector on the platform.

ACKNOWLEDGMENT The authors wish to thank the Alsace Region for the financial support of this research work.

REFERENCES

[1] Gangi, A., and Dietemann, J.-L., 1994. *Tomodensimétrie Interventionnelle*. Editions Vigot, PARIS.

[2] Stoianovici, D., Cadeddu, J. A., R. D. Demaree, H. A. B., Taylor, R. H., Whitcomb, L. L., and Kavoussi, L. R., 1997. "A novel mechanical transmission applied to percutaneous renal access". *Proceedings of the ASME Dynamic Systems and Control Division,* **DSC-Vol. 61** , pp. 401–406.

[3] Yanof, J., Haaga, J., et al., 2001. "CT-integrated robot for interventional procedures: Preliminary experiment and computer-human interfaces". *Computer Aided Surgery,* **6** , pp. 352–359.

[4] Fichtinger, G., DeWeese, T. L., Patriciu, A., Tanacs, A., Mazilu, D., Anderson, J. H., Masamume, K., Taylor, R. H., and Stoianovici, D., 2002. "Robotically assisted prostate biopsy and therapy with intra-operative CT guidance". *Journal of Academic Radiology,* **9** , pp. 60–74.

[5] Maurin, B., Piccin, O., Bayle, B., Gangloff, J., de Mathelin, M., Zanne, P., Doignon, C., Gangi, A., and Soler, L., 2004. "A new robotic system for CT-guided percutaneous procedures with haptic feedback". In Proceedings of the 2004 Computer Assisted Radiology and Surgery Congress (To appear), CARS'04.

[6] Simone, C., and Okamura, A. M., 2002. "Modeling of needle insertion forces for robot-assisted percutaneous therapy". In Proceedings of the 2002 IEEE International Conference on Robotics and Automation, ICRA'02, pp. 2085–2091.

[7] Maurin, B., Barbe, L., Bayle, B., Zanne, P., Gangloff, J., de Mathelin, M., Gangi, A., and Forgionne, A., 2004. "In vivo study of forces during needle insertions". In Proceedings of the 2004 Medical Robotics, Navigation and Visualisation Scientific Workshop (To appear), MRNV'04.

[8] Hunt, K., 1978. *Kinematic Geometry of Mechanisms*. Oxford Engineering Series, Clarendon Press.

[9] Tsai, L. W., 2001. *Mechanism Design : enumeration of kinematic structures according to function*. Mechanical Engineering series. CRC Press.

[10] Khalil, W., and Kleinfinger, J., 1986. "A new geometric notation for open and closed loop robots". In Proceedings of the 1986 IEEE International Conference on Robotics and Automation, pp. 75–79.

[11] Murray, R. M., Li, Z., and Sastry, S. S., 1994. *A Mathematical Introduction to Robotic Manipulation*. CRC Press.

[12] Park, F. C., 1994. "Computational aspects of the product-of-exponentials formula for robot kinematics". IEEE Transactions on Automatic Control, **39** (3) March , pp. 643–647.

[13] Yang, G., Chen, I. M., Lim, W. K., and Yeo, S. H., 1999. "Design and kinematic analysis of modular reconfigurable parallel robots". In Proceedings of the 1999 IEEE International Conference on Robotics and Automation, pp. 2501–2506.

[14] Smith, R., 2003. Open dynamic engine. web page: http://ode.org/.